The Astronomical Journal, 153:219 (12pp), 2017 May https://doi.org/10.3847/1538-3881/aa6899
© 2017. The American Astronomical Society. All rights reserved.

First Lensed Quasar Systems from the VST-ATLAS Survey: One Quad, Two Doubles, and Two Pairs of Lensless Twins*

Paul L. Schechter[1,4], Nicholas D. Morgan[2], B. Chehade[3], N. Metcalfe[3], T. Shanks[3], and Michael McDonald[1,4]
[1] MIT Kavli Institute for Astrophysics and Space Research, Cambridge, MA 02139, USA
[2] Staples High School, Westport, CT 06880, USA
[3] Durham University, Durham DH1 3LE, England
Received 2016 July 25; revised 2017 March 20; accepted 2017 March 20; published 2017 April 19

Abstract

We have analyzed images from the VST-ATLAS survey to identify candidate gravitationally lensed quasar systems in a sample of *WISE* sources with $W1 - W2 > 0.7$. Results from follow-up spectroscopy with the Baade 6.5 m telescope are presented for eight systems. One of them is a quadruply lensed quasar, and two are doubly lensed systems. Two are projected superpositions of two quasars at different redshifts. In one system, two quasars, although at the same redshift, have very different emission line profiles and constitute a physical binary. In two systems, the component spectra are consistent with the lensing hypothesis, after allowing for microlensing. However, as no lensing galaxy is detected in these two systems, we classify them as *lensless twins*. More extensive observations are needed to establish whether they are in fact lensed quasars or physical binaries.

Key words: gravitational lensing: micro – gravitational lensing: strong – quasars: general

1. Introduction

Doubly and quadruply lensed quasar systems are valuable for widely disparate purposes. Treu & Marshall (2016) present a current survey of the use of time-delay measurements for cosmography. The microlensing of lensed quasars can be used to determine sizes for the emitting regions of quasars (Rauch & Blandford 1991; Agol & Krolik 1999; Pooley et al. 2007; Blackburne et al. 2011) and to measure the dark matter fraction in lensing galaxies (Schechter & Wambsganss 2004; Pooley et al. 2012; Jiménez-Vicente et al. 2015). For each of these efforts the accuracy achieved is limited by the relatively small number of lensed systems.

The most productive lensed quasar discovery program to date has been the Sloan Digital Sky Survey Quasar Lens Search, henceforth SQLS (Inada et al. 2012), which yielded a statistical sample of 26 lensed quasar systems brighter than a limiting magnitude $i_{\rm lim} = 19.1$ over 8000 square degrees in the redshift range $0.6 < z < 2.2$. An additional 36 systems that did not satisfy all of the selection criteria were also cataloged. Of 62 systems in toto, 40 were newly identified.

The ATLAS survey, carried out with VLT Survey Telecope (Shanks et al. 2015), promises to yield comparable if not greater numbers of lensed quasar systems. Its *ugriz* limiting magnitudes are nearly identical to those of SDSS. While its *ugriz* photometry covers only 4500 square degrees, the typical ATLAS seeing is 3/4 that of SDSS (Shanks et al. 2015), permitting the discovery of quasar pairs with smaller separations.

We have undertaken a search for lensed quasars in the ATLAS survey, and report here the first newly discovered lensed quasars: a quadruple system, and two doubly lensed quasars. We also report two systems that have two nearly identical quasar spectra, but for which no lensing galaxy has been detected.

In Section 2 we outline our method for identifying candidate lensed quasar systems, using the *WISE* catalog and ATLAS *ugriz* cutouts to choose candidates for spectroscopic and direct imaging follow-up. The method will be described in greater detail in a forthcoming paper. In Section 3 we describe direct imaging and spectroscopic follow-up observations of seven cadidate systems obtained with IMACS on the Baade 6.5 m telescope of the Magellan Observatory. In Section 4 we analyze these observations. In Section 5 we present simple models for the the newly discovered quadruple system, WISE 2344-3056, and for one of the doubles, WISE 2304-2214. We discuss our method and results in Section 6 and summarize our findings in Section 7.

2. Selection of Candidate Lensed Quasar Systems

2.1. Colors for Marginally Resolved Lensed Quasar Systems

The colors derived for an object from a survey like ATLAS involve a number of implicit assumptions. Bright objects that are deemed point sources are used to determine a point-spread function (PSF) appropriate to the exposure, usually dominated by the atmospheric seeing. Sources that appear extended with respect to this PSF might be fit with a Sérsic (1963) profile. For sources that do not appear to be extended, one uses the adopted PSF to calculate a magnitude.

A gravitationally lensed quasar system is a composite object consisting of multiple images of a quasar and one or more lensing galaxies. Typical image separations are $\sim 1''$, to within a factor of two. It is unfortunate that the typical seeing in a survey like ATLAS is also on the order of one arcsecond. Were it very much better, one would detect the components of the lensed quasar as distinct objects and compute colors for each. Were it very much worse, one might treat the system as a point source.[5]

* This paper includes data gathered with the 6.5 m Magellan telescopes located at Las Campanas Observatory, Chile.
[4] MIT Department of Physics.

[5] One might in principle convolve survey images with a broadening function, perhaps blurring those taken in different filters to a common PSF, and produce a catalog for the smeared data, but only with the expenditure of considerable resources.

When the resolution of a survey is *comparable* to the image separation, the magnitudes derived for composite systems suffer systematic errors from the mismatch between the assumed PSF and the object. Moreover, these systematic errors will vary with the seeing. While one might hope to select lensed quasars using their cataloged colors, systematic errors may cause systems to be missed.

The resolution of the *WISE* survey (Wright et al. 2010) is substantially worse than that of ATLAS, and *WISE* magnitudes for all but the widest lensed quasar systems do not suffer from marginal resolution. Our approach is therefore to make a first level selection based only on *WISE* colors. This produces a candidate list sufficiently small that one can then retrieve the ATLAS survey images for each remaining source. The survey images can then be analyzed to determine whether two or more objects are present. Magnitudes are then computed by adopting a fixed configuration for all filters with the same number of components, thereby mitigating the systematic errors associated with marginally resolved systems.

2.2. W1 – W2 Color Selection

Stern et al. (2012) have shown that the *WISE* $W1 - W2$ color ($m_{3.6\mu} - m_{4.5\mu}$) can be used to isolate quasars from stars, and to a lesser extent, from galaxies. The underlying explanation is that the optical light from a quasar is thermal emission from an extended region with a range of temperatures, in which case the red tail of the distribution is redder than a blackbody Rayleigh-Jeans spectrum, which has $W1 - W2 \approx 0$ in the Vega system. We adopted a criterion, $W1 - W2 > 0.70$, that struck a balance between including lensed quasar systems and isolating them from other objects. Eighty percent of the confirmed SQLS lensed quasar systems satisfy this criterion. Lensing galaxies have bluer $W1 - W2$ colors than quasars. Systems in which the light from the lens dominates that of the quasars will not be included in our sample. The fraction of SQLS quasar systems that are bluer than our criterion is larger for the fainter systems. To keep the number of candidates manageable, we limited our sample to objects with $W1 < 15$ or $W2 < 14.45$.

In the south galactic cap, ATLAS covers a region with $21^h30^m <$ R.A. $< 4^h00^m$ and $-40° <$ decl. $< -10°$ in the *ugriz* filters with $0\farcs213$ pixels. (Shanks et al. 2015). In the north it covers[6] a region with $10^h00 <$ R.A. $< 15^h30^m$ and $-20° <$ decl. $< -2.5°$. The completed survey will include 4292 fields, each one degree square, located on $0\fdg98$ centers. As of mid-2016 March, there were 3650 fields for which data in *u*, *g,* and two or more of *r*, *i,* and *z* were available.

ATLAS survey data in at least one filter were available, as of 2016 mid-March, for 144,700 unique sources that satisfied our *WISE* criteria.

2.3. Cutouts

For each source in the overlap between *WISE* and ATLAS we downloaded $12''$ square *ugriz* FITS subrasters (58 pixels on a side) from the University of Edinburgh Wide Field Astronomy Unit's OmegaCam Science Archive (henceforth OSA; Hambly et al. 2008; Cross et al. 2012). The size of these "cutouts" was chosen to be larger than most known quasar/galaxy lens systems while minimizing the possibility of including an unrelated source in the field.

2.4. Splitting Blended Images

For each source the available cutouts were analzyed with a program that incorporates many of the core subroutines from the DoPHOT photometry program (Schechter et al. 1993). DoPHOT uses an elliptical profile that approximates a Gaussian near the core, but it has broader wings.

In each of the three filters with the best seeing, as recorded in the FITS header of the cutout, we attempt to split candidates into two sources with a common quasi-Gaussian shape. From these we chose the two-source fit that shows the greatest improvement over a single extended object (as measured by our goodness-of-fit parameter) as our "anchor" estimate of the separation between components.

For as many of the *ugriz* filters as we have cutouts, we carry out two-source fits, with the separation constrained to our anchor value, but allowing the fluxes to vary along with a common set of shape parameters and an overall position. We call these constrained separation fits.

If the flux ratio from one of these constrained separation fits is very different from the anchor value (3 mag) at a high level of significance (10σ), we take the anchor splitting to be spurious. This frequently happens at smaller separations, at which trailed or astigmatic images can cause the object to look elongated or double in one exposure.

2.5. Weeding Out Galaxies

In addition to quasars, our *WISE* quasar-colored systems include star-forming galaxies, which often come in close pairs. Moreover, with a thousand unlensed quasars for every lensed quasar, we expect accidental projections of foreground galaxies close to quasars.

Every constrained separation fit gives us an elliptical footprint that can be compared with the seeing as recorded in the FITS header for that filter. Pairs of galaxies are expected to have larger footprints, as measured by the area of the quasi-Gaussian, than the stellar PSF. After some experimentation, we decided to eliminate as a probable galaxy pair any system for which the *area* of the constrained separation footprint is larger than that of the stellar PSF by 2 pixels in all three of the filters with the best seeing.

We carry out a second test using the cutout that yielded our anchor splitting, fitting for two sources whose shapes are not constrained to the same elliptical Gaussian. This adds three additonal shape parameters, but the fits converge for roughly 65% of our candidates.

We exclude systems for which the minor axes of the two components differ by more than than a factor of $\sqrt{2}$. We reason that while our splitting might lump together a close pair of quasar images, or a quasar image and the lensing galaxy, the minor axis of the fitted ellipse ought not to be much larger than the PSF of a star. Instead of using a nominal PSF, however, we use the fit to the other split component. We further tighten this criterion if the major axis of the wider component is very much larger than the narrower component, excluding systems for which the minor axes differ by more than a factor of $2^{1/4}$ and for which the ratio of the areas is larger than a factor of two.

[6] A second northern region with $10^h00^m <$ R.A. $< 15^h00^m$ and $-35° <$ decl. $< -20°$ is being surveyed in *i* and *z*, with *u*, *g*, and *r* being observed in a separate ESO program (095.A-0561, PI L. Infante), but was not included in the present search.

Table 1
Spectroscopic Observations of Lensed Quasar Candidates

name	R.A. Decl.	$\Delta\theta$ P.A.	i_A[a] i_B[a]	Score $(u-g)$[b]	Camera Exp.	Description Redshift (A/B)
WISE 0145-1327	01 45 25.3 −13 27 25	1.″68 5°	19.25 20.59	0.39 −1.01	$f/2$ 1200s	projected 1.09/1.97
WISE 0326-3122	03 26 06.8 −31 22 54	1.″43 −60°	19.49 20.56	0.60 −1.17	$f/2$ 1200s	lensless twins 1.34
WISE 1051-1142	10 51 41.9 −11 42 39	1.″47 −5°	17.25 19.39	0.50 −0.89	$f/4$ 900s	lensless twins 0.88
WISE 1427-0715	14 27 04.8 −07 15 56	2.″80 9°	18.92 20.32	0.49 −0.73	$f/4$ 900s	projected 1.23/0.72
WISE 2215-3056	22 15 25.6 −30 56 35	0.″71 −41°	18.31 19.07	0.29 −0.61	$f/4$ 900s	binary 1.34
WISE 2304-2214	23 04 25.3 −22 14 46	2.″19 −11°	19.57 20.50	0.58 −1.37	$f/4$ 1800s	lensed 1.42
WISE 2329-1258	23 29 57.9 −12 58 59	1.″27 46°	17.63 18.60	0.96 −0.82	$f/2$ 600s	lensed 1.314
WISE 2344-3056	23 44 17.0 −30 56 26	2.″18 −12°	20.31[c] 20.63[c]	0.44 −0.63	$f/2$ 900s	quadruple 1.298

Notes.
[a] magnitudes for A and B components derived from cataloged ATLAS Petrosian AB magnitudes and constrained separation flux ratios.
[b] $u-g$ colors are in the Vega-like system of the ATLAS FITS headers.
[c] $i_C = 20.71$ and $i_D = 21.12$.

2.6. Ranking on the Basis of Achromaticity

The word "achromatic" is often used to describe gravitational lensing. While color may vary from one part of an extended source to another, if the source is small compared to the Einstein ring of a gravitational lens, the multiple images will all have the same color.

This is less powerful than one might hope in discriminating between lensed quasar systems and chance superpositions of objects for two reasons. First, lensed systems also include lensing galaxies, the light from which will be split disproportionately between the two images. Second, especially at brighter apparent magnitudes, the quasars are microlensed by the stars within the lensing galaxies and are somewhat extended compared to the microlensing Einstein rings. This leads to differential microlensing (Blackburne et al. 2011).

We use the constrained separation flux ratios at each observed wavelength, expressed in magnitudes, δm_λ, to fit for a slope, $d\delta m_\lambda / d\log\lambda$. We adopt a rough guess of the mean slope for a lensed system $\langle\alpha\rangle = 0.217$, and of the scatter in that slope, $\sigma_\alpha = 0.325$, and score systems based on their deviation from the mean slope.[7] We also score systems on the absence of scatter from the observed slope and finally score systems on the consistency of the u filter flux ratio with those in the other filters. A final ranking is computed by taking the geometric mean of these three scores. Details of our scoring system (which we continue to refine as we observe more candidates) will be presented in a forthcoming paper.

[7] The mean slope is non-zero because fainter images are more likely to include more of the red light from the lensing galaxy.

2.7. Optical Colors

We have argued above that cataloged optical colors may be unreliable for lensed quasar systems because catalog photometry explicitly or implicitly assumes a light distribution over the detector pixels that is inappropriate for a lensed quasar system. Our constrained separation model should produce better (but hardly perfect) colors.

For this our first pass through the data, we restricted ourselves to the simplest of quasar color criteria, ultraviolet excess (henceforth UVX). This works well for quasars with $z < 2.2$ (Richards et al. 2001), but would exclude the roughly 25% of unlensed quasars in an SDSS-like survey that have higher redshifts.

Optical colors were computed by adding the two fluxes from the constrained separation fits in each of the filters. The photometric zeropoints embedded in the OmegaCam FITS headers were used to create $u-g$ colors in a Vega-like *ugriz* system (Shanks et al. 2015). We ultimately adopted $u - g < -0.5$ as our UVX criterion, which seems to exclude narrow emission line galaxies and white dwarf pairs, but does include lensed quasars at $z < 2.2$.

After applying the recipe described in this section, we are left with a ranked list of candidate lensed quasar systems.

3. Spectroscopic and Direct Observations and Reductions

From 2015 June through 2016 April and again in 2016 November, spectroscopic observations were carried out for roughly a dozen highly ranked systems with both the $f/2$ and $f/4$ cameras of the Inamori Magellan Areal Camera and Spectrometer, henceforth IMACS (Dressler et al. 2011) on the Baade 6.5 m telescope of the Magellan observatory. In Table 1

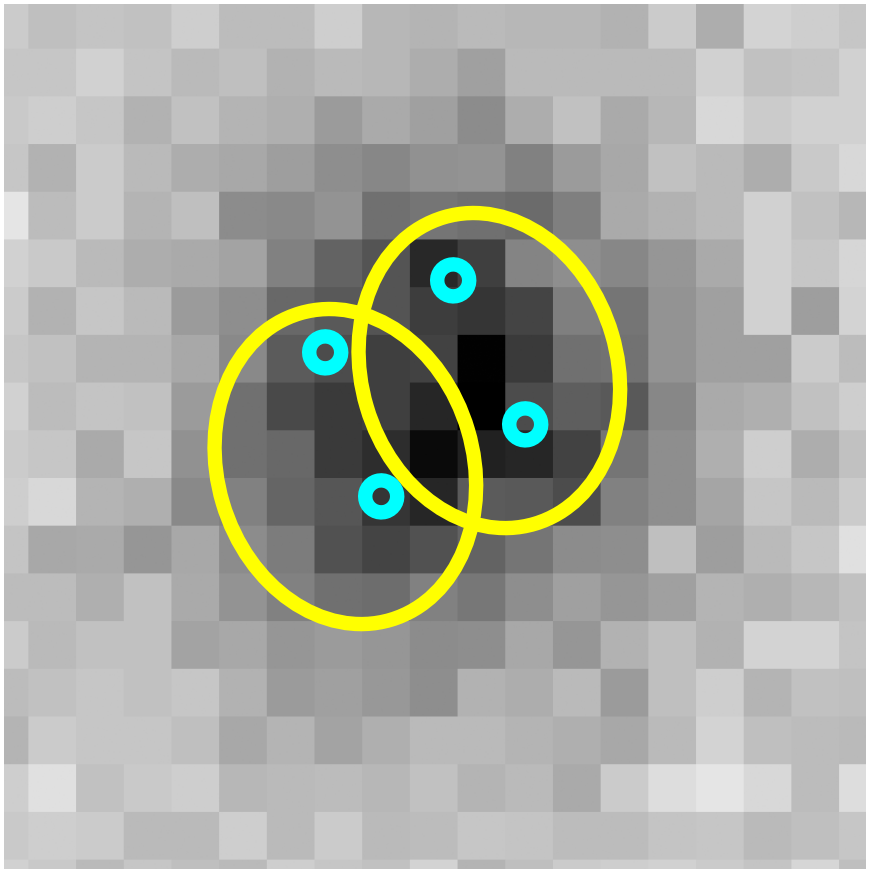

Figure 1. VST-ATLAS *g* stack for WISE 2344-3056. The yellow ellipses are the result of our anchor splitting of this source. The blue circles are at the positions of the four images (D, C, B, and A from left to right) identified with IMACS. The scale is $0\farcs213$ per pixel. North is up and east is to the right.

we give coordinates for eight of the objects observed, their rankings and colors, and descriptions of the resulting spectra.

3.1. Choice of Systems

While guided by rank, the actual choice of systems to observe also depended upon seeing, as some of the systems are quite close, and upon cloud cover. Pairs of blue stars and narrow-line galaxies with $-0.5 < u - g < 0$ that predominated in our first observations led us to tighten our UVX criterion to $u - g < -0.5$ in subsequent runs.

3.2. Direct Imaging of WISE 2344-3056

The system WISE 2344-3056 was given top priority for observation in 2015 December because its appearance in the ATLAS images suggested a quadruple system. Figure 1 shows the VST-ATLAS image of WISE 2344-3056 in the *g* filter, which gave the best splitting of the object. We have superposed the elliptical FWHM contours from the anchor fit to this image.

The minor axis of the anchor fit is $1\farcs11$, slightly less than the $1\farcs18$ seeing reported in the image header. The major axis is $1\farcs41$ and elongated so that each ellipse includes two of the four images.

The system only barely survived being eliminated as a pair of galaxies, suggesting that we may need to relax the constraint on the area of the anchor footprint described in Section 2.5.

The spectrocopic mode used with IMACS required the taking of one or more short direct images to position the object in the slit. The first of those obtained for WISE 2344-3056, in Sloan *r*, confirmed the suspicion that it was at least triple. Two more images were therefore taken in Sloan *i*. The left panel of Figure 2 shows one of the *i* images, taken in $0\farcs55$ seeing with the $f/2$ camera.

The debiased and flatfielded frames were analyzed using the program DoPHOT (Schechter et al. 1993). The standard version of the program found all four quasar images on the *r* frame and needed only minor adjusting to find all four on the other two. The right panel of Figure 2 shows the residuals from one of those fits, using the point-spread function of a nearby star as the empirical PSF. While the residuals show little or no trace of a lensing galaxy, the figure is somewhat deceptive. If one allows for a *fifth* point source with its position fixed at the expected position of the lens (see Section 5 below), the magnitudes of the four quasar images decrease by hundredths of a magnitude, the positions spread out radially by roughly 0.1 pixel each, and the flux from the hypothesized fifth image is 1.5 ± 0.5 magnitudes lower than that of image D.

Astrometry was carried out on one of the *i* frames using cataloged positions from the ATLAS survey, with rms residuals of $0\farcs1$. Results are given in Table 2. The four positions are indicated by the blue circles in Figure 1.

Fluxes relative to the brightest image were likewise computed using DoPHOT. These were then used to compute magnitudes assuming a combined Petrosian *i* magnitude of 19.15 as given in the ATLAS catalog, which reports magnitudes in an AB system (Shanks et al. 2015) rather than in the Vega-like system of the FITS headers. To the extent that

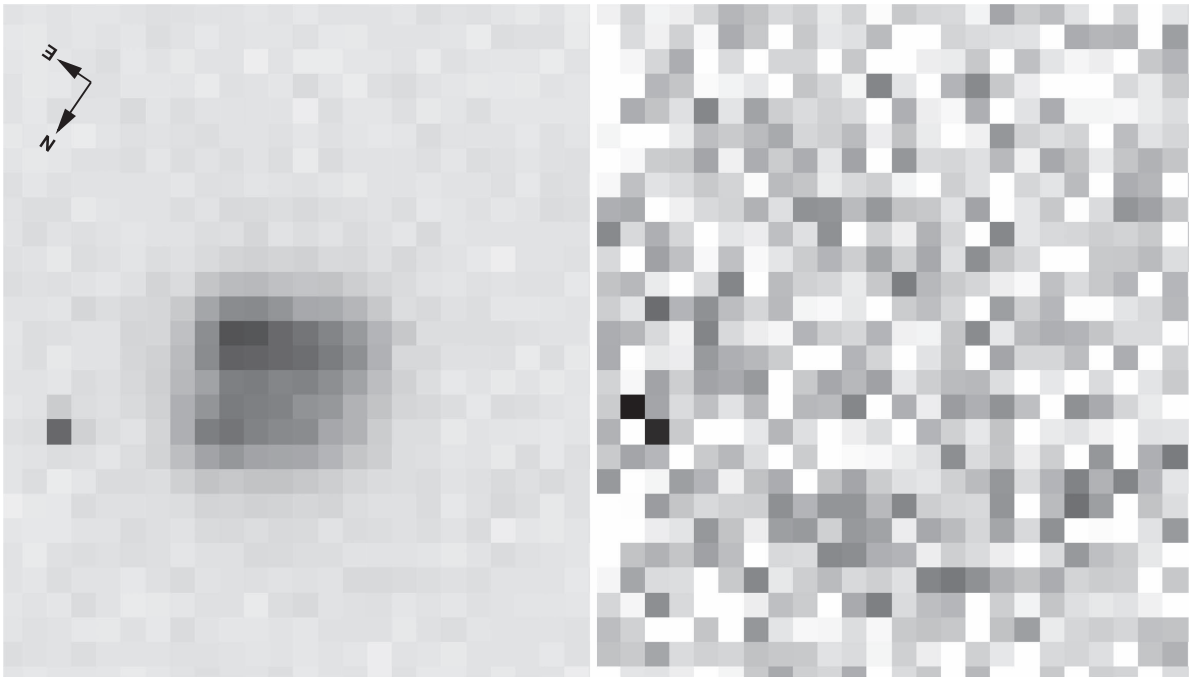

Figure 2. Left: 60s *i* exposure of WISE 2344-3056 taken with IMACS in 0.″55 seeing. Right: the same exposure, with four point sources subtracted, at 10 times higher contrast. The scale is 0.″200 per pixel.

Table 2
Astrometry[a] and Photometry for WISE 2344-3056

image	$\Delta\alpha$	$\Delta\delta$	i
A	0.″000	0.″000	20.31
B	−0.″304	0.″665	20.63
C	−0.″641	−0.″337	20.71
D	−0.″886	0.″293	21.12

Note.
[a] Positions in arcseconds relative to $\alpha_A = 23^h44^m16.″995$ and $\delta_A = -30°56'26.″22$.

the quasar has varied in the four years between the ATLAS and IMACS exposures, these will share a common systematic error.

3.3. Direct Imaging of WISE 0326-3122

A 30s direct image of WISE 0326-3056 in the Sloan *r* filter in 0.″64 seeing was obtained with the IMACS *f*/2 in acquiring the object for spectroscopy. The debiased and flatfielded frame was analyzed with DoPHOT. Figure 3 shows the original image of the candidate system and the same image with best-fitting PSFs subtracted. The residuals show little or no trace of a lensing galaxy. In contrast to the case of WISE 2344-3056, the residuals are not deceptive. If one allows for a *third* point source with its position fixed near the expected position of the lens (one third of the way from the fainter image to the brighter image), one obtains a *negative* flux with an amplitude that is only 1% of the amplitude of the fainter image. This limit is sensitive to the assumed position for the lens, which, as we see in the case of WISE 2304-2214 below, can be quite different from the expectation.

3.4. Direct Imaging of WISE 2304-2214

In setting up for spectroscopy of WISE 2304-2214, a 30s acquisition image in the Sloan *r* filter was obtained in 0.″63 seeing with the IMACS *f*/4 camera binned 2 × 2. There appeared to be a lensing galaxy in between two pointlike images. A 60s image in the Sloan *i* filter was therefore obtained following spectroscopy. Both exposures were analyzed by fitting two scaled versions of a stellar template and a quasi-Gaussian. The separations determined from the *i* exposure were enforced on the *r* exposure.

Figure 4 shows the original Sloan *i* image, the same image with all three sources subtracted, at 10 times the contrast, and again with only the two point sources subtracted at four times the contrast. We take the central object to be the lensing galaxy. The scale is 0.″221 per pixel.

In Table 3 we give positions and magnitudes for all three sources. The latter are derived from the cataloged ATLAS magnitudes for the stellar templates, two of which were used for each filter. The quasi-Gaussian fit yields shape paramters for the lensing galaxy. We deconvolve that quasi-Gaussian using a similar fit to the template star and find the semimajor and semiminor axes to be 0.58 and 0.25 pixels, respectively, at position angle −68.°6, which is 9.°5 off the pependicular to the line connecting the two images. Similar results were obtained from the *r* exposure. It is noteworthy that contrary to the expectation for simple isothermal sphere models, the lensing galaxy is closer to the brighter image. In this regard, it is similar to the case of HE1114-1805 discussed in Section 4.1 below.

3.5. Spectra

Spectra for the objects in Table 1 were obtained using either the "short" *f*/2 camera or "long" *f*/4 camera on IMACS, in both cases using a 3800–7000 Å blocking filter. Dispersers with 300 lines mm^{-1} were used on both cameras: a grism blazed at 17.°5 on the short camera and a grating blazed at 4.°3

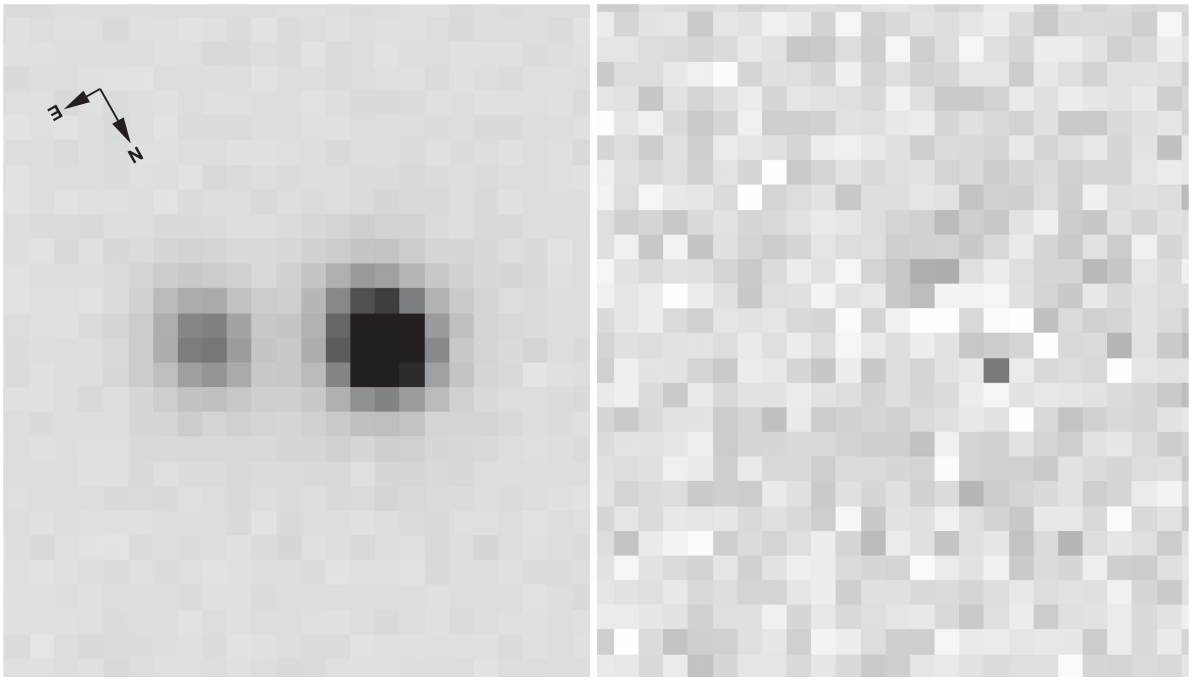

Figure 3. Left: 30s Sloan *r* exposure of WISE 0326-3122 in 0.″64 seeing. Right: the same exposure, with two point sources subtracted, at five times higher contrast. The scale is 0.″200 per pixel.

on the long camera. On the short camera, the spectra were binned by 2 pixels in the spectral direction (except where noted). On the long short camera, they were binned by 4 pixels in the spectral direction and 2 pixels (with one exception) along the slit. The 0.″9 slit was oriented to obtain spectra of both components of the double systems.

The spectra were bias-subtracted and flattened using standard procedures, and cosmic rays near the extraction paths were identified by eye and replaced with interpolated values along each row of the detector. Wavelength calibration was provided by Argon lamp lines taken during the afternoons. A multi-order polynomial fit as a function of both the spatial and dispersion directions was used for the wavelength solution and gave typical fit rms values with respect to the reference line list of 0.3 Å or better for all target chips. The dispersion ranged from 2.2 to 2.6 Å pixel^{-1} on the short camera and from 2.8 to 3.0 Å pixel^{-1} on the long camera. Sky background was subtracted using linear interpolation along each row of the detector. The spectra show gaps near 6550 Å on the short camera and near 5300 Å on the long camera, which is due to the physical spacing between CCDs on the IMACS cameras.

When the seeing permitted, spectra were extracted for the individual components of each system. The was accomplished by fitting multiple overlapping Gaussian profiles to each spatial row of the detector. We performed a preliminary fit for each row to obtain average component separations, and then a final extraction where the overall position, common FWHM, and component brightnesses were allowed to vary, but the relative separations were fixed at the average values.

Figures 5–7 show the extracted spectra for the objects in Table 1; note that no flux calibration was performed. The displayed spectra were top-hat smoothed using a 3-pixel window in the dispersion direction for cosmetics. Gaussian profile fitting was performed on the unsmoothed spectra, and we plot the base-10 log of our fitted Gaussian profile areas along the ordinate. We were able to extract individual spectra for WISE 0145-1327, WISE 0326-3122, WISE 1051-1142, WISE 1427-0715, WISE 2215-3056, WISE 2304-2214, and WISE 2329-1258. For these systems an inset at the lower right of each plot shows the Gaussian decomposition of the two components for a single CCD row of the detector. The small separation of WISE 2344-3056 precluded decomposing the spectra. A single Gaussian was therefore used to extract the combined spectrum.

4. Interpretation of Spectra

4.1. Binary Quasar, Lensed Quasar, or Lensless Twins?

The words "binary quasar" are used to describe two distinct quasars at the same redshift, as opposed to two images of a lensed single quasar (Hennawi et al. 2006). When one observes a pair of quasars, however, conclusive discrimination between these two alternatives is not always straightforward (Wisotzki et al. 1993; Kochanek et al. 1999; Mortlock et al. 1999).

The history of HE1104-1805 is instructive in this regard. Wisotzki et al. (1993) found that the two components differed in the slopes of their continuua and in the equivalent widths of their emission lines, but that the shapes of their emission lines were identical. They argued that the spectral differences might be due to microlensing by stars in the lensing galaxy. However, they detected no lensing galaxy at $R \lesssim 24$. Wisotzki et al. (1995) subsequently observed correlated changes in the continuum flux of the two systems, which they took as confirmation of the lensing hypothesis. Courbin et al. (1998) conclusively detected the lensing galaxy, much closer to the brighter image than might naively have been expected. Crude interpolation between filters in subsequent *HST* observations (Remy et al. 1998) would give $R \sim 22$ for the lensing galaxy. Lidman et al. (2000) measured a lens redshift of $z = 0.729$.

The circumstances of two of our systems are similar to those of HE1104-1805 in 1993. The spectra differ, but no more than

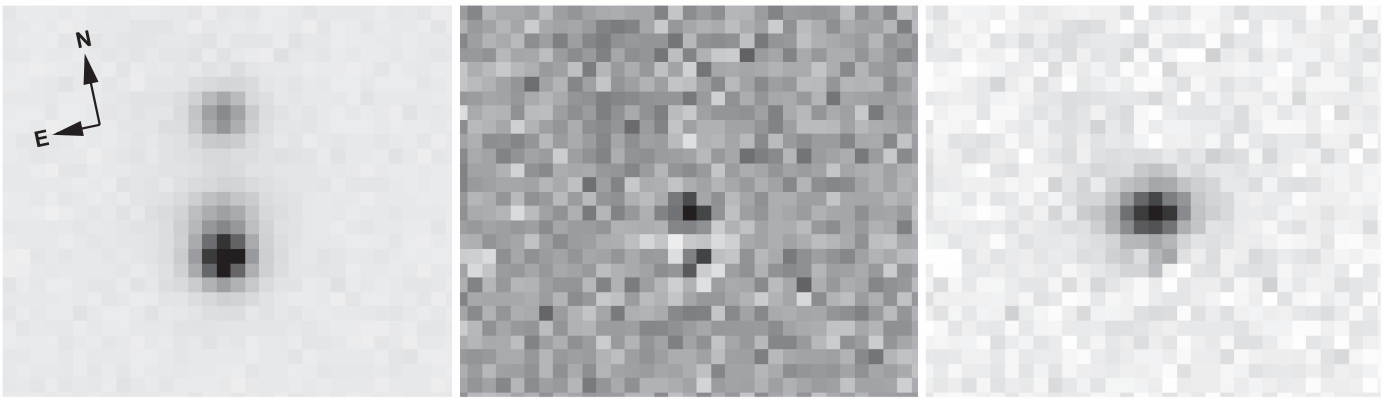

Figure 4. Left: 60s Sloan *i* exposure of WISE 2304-2214 in $0\farcs64$ seeing. Center: the same exposure, with two point sources and an extended source subtracted, at 10 times higher contrast. Right: the same exposure with only the point sources subtracted, at 4 times higher contrast. The scale is $0\farcs221$ per pixel.

Table 3
Astrometry[a] and Photometry[b] for WISE 2304-2214

image	$\Delta\alpha$	$\Delta\delta$	r	i
A	$0\farcs000$	$0\farcs000$	19.52	19.57
B	$-0\farcs431$	$2\farcs145$	20.46	20.50
G	$-0\farcs093$	$0\farcs673$	21.48	20.65

Notes.
[a] Positions in arcseconds relative to $\alpha_A = 23^h04^m25\farcs348$ and $\delta_A = -22°14'46\farcs95$.
[b] Magnitudes from three component fits to Magellan images with the scale set by ATLAS AB magnitudes for template stars.

they might under the microlensing hypothesis. Still, we observe no lensing galaxy. We think it premature to call such systems binary quasars, and instead refer to them as "lensless twins." If lensing galaxies or correlated variations are ultimately observed, they will be classified as lens systems.

When only upper limits can be measured for a lensing galaxy, however, careful modeling is needed to establish that these upper limits are inconsistent with plausible lensing scenarios. Alternatively, higher signal-to-noise spectra or spectra of narrow emission lines might show significant differences in the line profiles or redshifts, ruling out the lensed system hypothesis.

In the sequel to the SQLS, the SDSS-III BOSS Quasar Lens Survey, More et al. (2016) are similarly circumspect in not drawing strong conclusions about lensless twins for which no lensing galaxy is observed.

4.2. WISE 0145-1327: a Projected Pair

WISE 0145-1327 is a chance projection of two quasars. The brighter of the pair is at a redshift of $z = 1.0902 \pm 0.0005$ from a Gaussian fit to the Mg II emission line. The fainter object is at a higher redshift of $z = 1.9749 \pm 0.0005$ based on its CIV broad emission line. The spectra are shown in Figure 5.

4.3. WISE 0326-3122: Lensless Twins at $z = 1.34$

The two quasar images of WISE 0326-3122 have nearly identical redshifts and spectral flux ratios. Both show a C III] broad emission line at around 4460 Å. Gaussian fits to the C III] profiles yield identical source redshifts of $z = 1.3342 \pm 0.0016$ for the brighter object and $z = 1.3336 \pm 0.0026$ for the fainter object. This redshift places the Mg II broad emission line inside the IMACS chip gap with only a hint of the feature's wing visible for the brighter component. A Mg II $\lambda\lambda$2796, 2803 absorption doublet at $z = 0.5080 \pm 0.0001$ is also present in the brighter component's spectrum. The flux ratio between components is also remarkably constant at about 3.2:1 (0.5 dex in Figure 5) over the entire IMACS spectral range. This makes it all the more surprising that no lensing galaxy is observed in the PSF-subtracted image (Figure 3). We take the two sources to be lensless twins.

4.4. WISE 1051-1142: Lensless Twins at $z = 0.88$

The two quasar images of WISE 1051-1142 have nearly identical redshifts. The single prominent emission line just blueward of the IMACS chip gap is likely Mg II due to the absence of other emission features in the observed wavelength range. Gaussian fits to the emission profiles yield source redshifts of $z = 0.8839 \pm 0.0002$ and $z = 0.8811 \pm 0.0008$ for the brighter and fainter components, respectively, which overlap at the 3–4σ level. There are no obvious signs of intervening absorption. The flux ratio between components varies from 6:1 at the blue end to 7:1 at the red end, which is consistent with wavelength-dependent continuum microlensing seen in other lensed quasars. We take the two sources to be lensless twins.

4.5. WISE 1427-0715: a Projected Pair

WISE 1427-0715 is a chance projection of two quasars. The brighter component shows the Mg II broad emission line at about 6230 Å, which yields a source redshift of $z = 1.2258 \pm 0.0004$. The only prominent emission line at 4820 Å in the fainter component is likely Mg II because other features in the observed wavelength range are absent, which yields a source redshift of $z = 0.7218 \pm 0.0004$. A Mg II $\lambda\lambda$2796, 2803 absorption doublet is also seen in the brighter component's spectrum at a fitted redshift of $z = 0.7205 \pm 0.0004$, and thus it is associated with the host galaxy of the fainter quasar. The spectra are shown in Figure 6.

4.6. WISE 2215-3056: a Binary Quasar at $z = 1.34$

WISE 2215-3056 is a binary quasar. Its components have similar redshifts but notable spectral differences. The brighter component is at $z = 1.3474 \pm 0.0003$ based on its Mg II broad emission line profile and shows strong absorption features

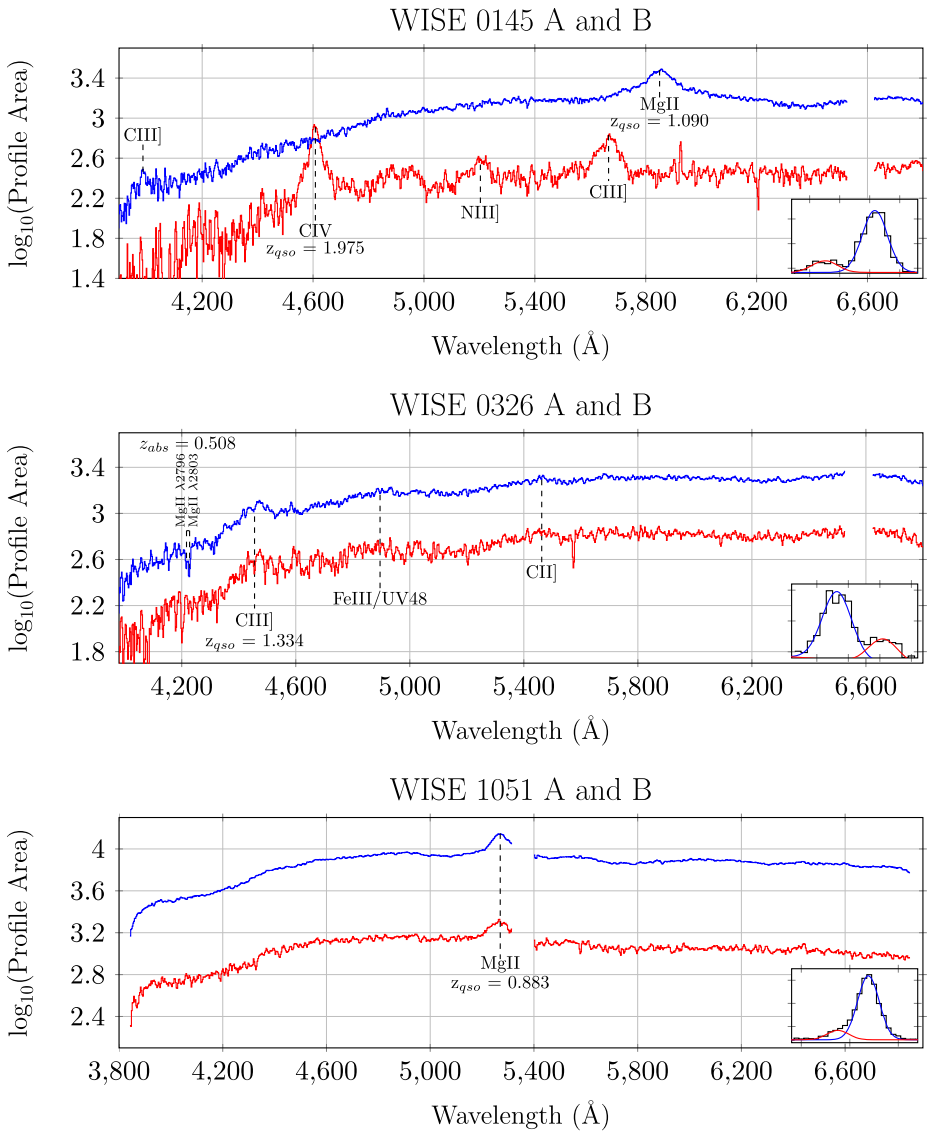

Figure 5. IMACS spectra of WISE 0145-1327, WISE 0326-3122, and WISE 1051-1142. Image A is brighter than image B.

blueward of its C III] and Mg II emission lines. The fainter component has a source redshift of $z = 1.3508 \pm 0.0004$ based on its Mg II profile, a $>5\sigma$ difference from the brighter component, but it shows neither of the two absorption features seen in the brighter component. There is also a prominent Fe III/UV 48 broad emission line of comparable intensity to C III] in the brighter component that is lacking in the fainter companion. Despite the similar redshifts, the spectral differences argue for two separate quasars. The spectra are shown in Figure 6.

4.7. WISE 2304-2214: a Doubly Lensed Quasar at z = 1.42

WISE 2304-2214 is a doubly lensed quasar at z = 1.423. The quasar spectra shown in Figure 6 have emission at C III], C II], and Mg II. Gaussian fits to the Mg II emission profiles yield source redshifts of $z = 1.4222 \pm 0.0004$ and $z = 1.4218 \pm 0.0003$ for the brighter and fainter components, respectively. The brighter component has a Mg II absorption doublet at $z = 0.6362 \pm 0.0001$ that is much weaker, if not totally absent, in the fainter component. Fitting a third Gaussian component of the same width between the two quasar components yields a spectrum of what appears to be the lensing galaxy with Ca H&K absorption near 5700 Å, giving $z_{\rm gal} = 0.4455 \pm 0.0004$.

The emission line equivalent widths are substantially smaller in the brighter component, suggesting that one or both components are microlensed. We make a crude estimate of emission line flux ratios by comparing the peak flux in the emission line to the flux in the adjacent continuum. We obtain emission line flux ratios of $B/A = 0.99$ for the C III] line and and $B/A = 1.06$ for the Mg II line.

4.8. WISE 2329-1258: a Doubly Lensed Quasar at z = 1.31

The two quasar images of WISE 2329-1258 have nearly identical redshifts with a rich set of absorption features present in both spectra, as shown in Figure 7. The Mg II broad emission line is at $z = 1.3077 \pm 0.0008$ for the brighter component and $z = 1.3174 \pm 0.0018$ for the fainter component, overlapping at the 5σ level. A similar agreement is seen for the C III] broad emission line. The narrow-line absorption

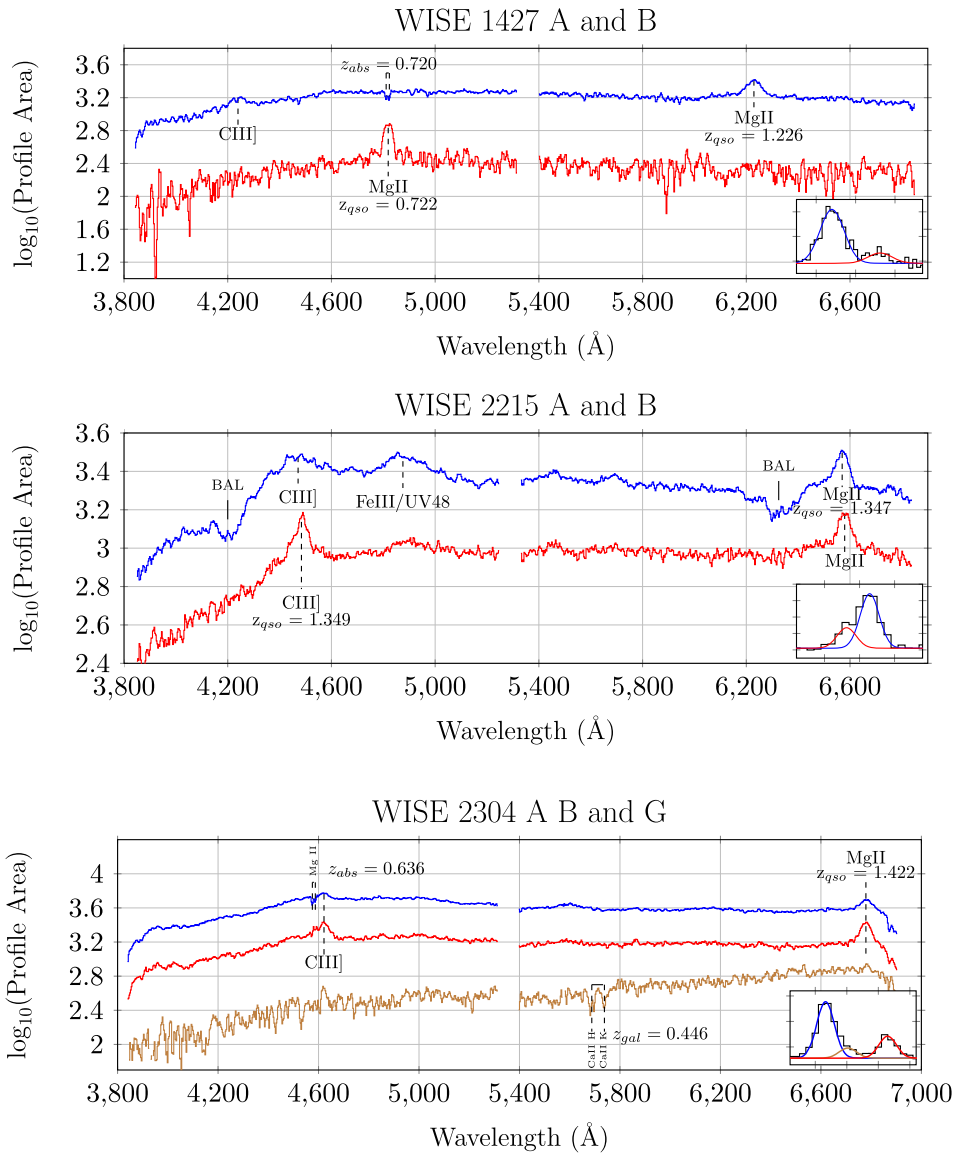

Figure 6. IMACS spectra of WISE 1427-0715 and WISE 2215-3056 and WISE 2304-2214. Image A is brighter than image B.

features present in the spectra of both components can be modeled with two absorbers at $z = 1.1525 \pm 0.0002$ and $z = 0.7644 \pm 0.0004$. Both are anchored by an appropriately redshifted Mg II $\lambda\lambda$2796, 2803 doublet and accompanying Fe II $\lambda\lambda$2382, 2600 absorption lines. We also identify Fe II $\lambda\lambda$2344, 2374, and 2586 for the $z = 1.1525$ absorber. The flux ratio between the components is also remarkably constant at about 2.5:1 (0.4 dex in Figure 7) over the entire IMACS spectral range.

Based on the Magellan data presented here, WISE 2329-1258 would be classified as a lensless twin system. T. Treu et al. (2017, private communication) have observed it using NIRC2 on Keck II behind adaptive optics, however, and detected the lensing galaxy as well as the lensed quasar host galaxy. We therefore count it as a confirmed lens. Like HE 1104-1805, this system also has strong absorption line systems, and we would not be surprised if one of them were the lens redshift.

4.9. WISE 2344-3056: a Quad at $z = 1.30$

The slit used to obtain a spectrum for WISE 2344-3056 ran along the line connecting the ellipses in Figure 1, with light from all four images overlapping on roughly six spatial pixels. We present only the combined spectrum in Figure 7. The quasar redshift is $z = 1.2978 \pm 0.0003$ based on a Gaussian fit to the Mg II broad emission line. The C III] broad emission line is also present at a much lower signal-to-noise ratio. There is at least one intervening absorption system at $z = 0.9472 \pm 0.0012$ anchored by the Mg II $\lambda\lambda$2796, 2803 absorption doublet, several Fe II lines ($\lambda\lambda$2344, 2374, 2382, 2399, 2586, 2600), Fe III λ2419, and MgI λ2852.

5. Lens Models

We used Keeton's `lensmodel` program (2001) to fit models to our astrometry for WISE 2304-2214 and WISE 2344-3056 given in Tables 2 and 3.

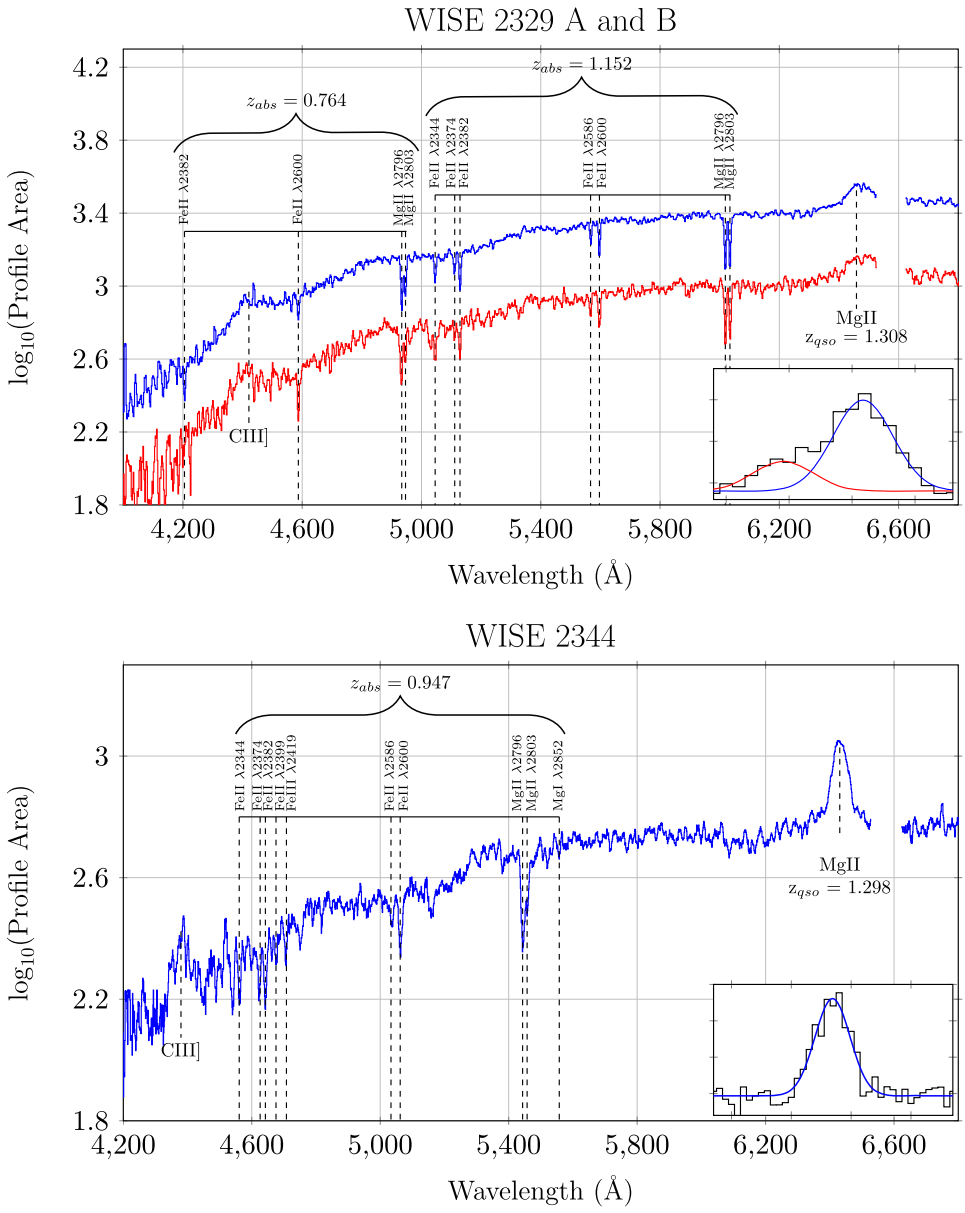

Figure 7. IMACS spectra of WISE 2329-1258 A (uper) and B (lower) and WISE 2344-3056, taken with IMACS.

5.1. WISE 2304-2214

For WISE 2304-2214 we used a singular isothermal ellipsoid. The generic expectation is that the quasar images will be microlensed (Witt et al. 1995), and we are reluctant to use their continuum flux ratos as constraints. As this leaves the model underconstrained, we took the emission line flux ratio to be approximately unity and adopted this as a constraint.

The model puts the source 0.″17 west and 1.″08 north of image A, and the source has a lens strength of 1.″04. The model magnifications are −2.6 and 2.6 for images A and B, respectively. By contrast, image A is 0.94 mag brighter than B in the *r* and *i* filters. We take this to be an indication of microlensing of the continuum. Image A is more likely to be microlensed than image B, both because A is a saddle point (Schechter & Wambsganss 2002) and because B is more than twice as far from the lensing galaxy and passes through a lower surface density of stars.

The model ellipticty is 0.22 and is directed along P.A. 73.°0 east of north, as compared to the observed ellipticity and orientation of 0.58 and 111.°4. Shear of 0.1 from a galaxy 5″ toward P.A. 30° from image B produces models with higher ellipticities that are more nearly aligned with the observation.

5.2. WISE 2344-3056

For WISE 2344-3056 we used a singular isothermal sphere with external shear to fit astrometric data in Table 2. As we do not detect the lensing galaxy, the center of the lens is left free and found to be 0.″436 west and 0.″151 north of image A. The model places the source 0.″441 west and 0.″153 north of image A. The lens strength—which would be the radius of the Einstein ring

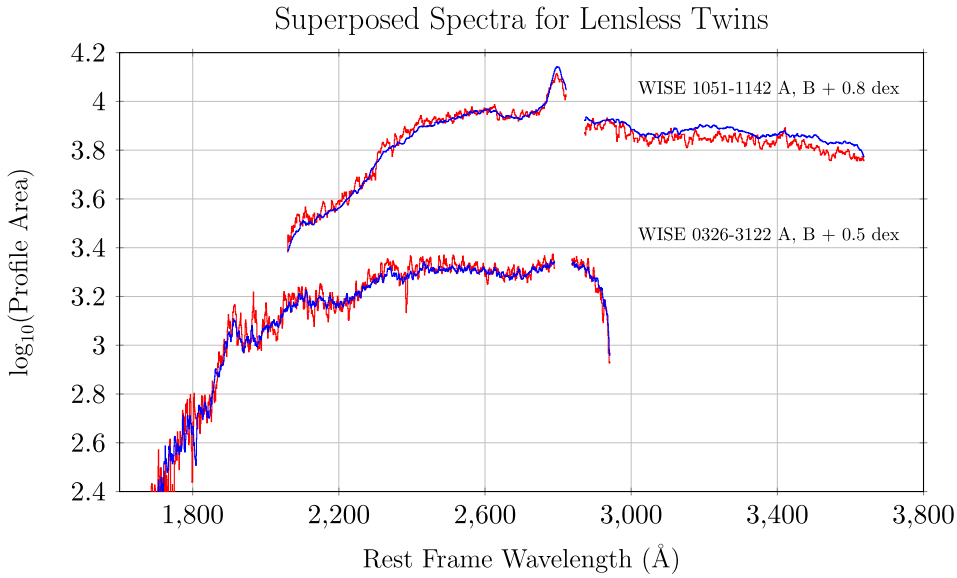

Figure 8. Rest-frame spectra of WISE 0326-3122 and WISE 1051-1142 with the *A* and *B* components superposed.

were there no shear—is 0.″99. The external shear is 0.063 and is directed along P.A. −71.°5. The signed magnifications for images A, B, C, and D are −6.8, 8.4, 8.6, and −8.1, respectively.

6. Discussion

6.1. The Method

We have searched for gravitationally lensed quasars by analyzing VST-ATLAS image cutouts of red *WISE* sources. Those that could be consistently split into two nearly pointlike objects with roughly constant flux ratios across multiple filters and quasar-like colors in these filters (specifically $u - g < -0.5$) were selected as candidates for follow-up spectroscopy and imaging. Three new lenses, two pairs of lensless twins, one binary quasar, and two projected quasar pairs were found. Owing to bad weather during 2015 and 2016, only a fraction of the candidates (albeit some of the best) were observed.

The list of candidates is likely to increase considerably with (a) completion of the ATLAS survey, (b) application of the method to fainter *WISE* sources, and (c) incorporation of a more sophisticated scheme for gauging whether the *ugriz* colors of a particular pair of objects are quasar-like. The method could be extended to splitting sources into triples, with the primary goal of more readily identifying quadruply lensed quasars.

We encountered an unanticipated bottleneck in the speed with which the OmegaCam Science Archive can produce cutouts—something on the order of one cutout per second, far more than one might think necessary for retrieving 2500 pixels. The servers for the DES and KiDS surveys are not qualitatively faster. This casts a pall on programs that might require 10^7 or 10^8 cutouts. While it might be difficult to retool existing archives to speed up the process, we imagine that future systems will deal with such programs more efficiently.

Our method (modified for use with *grizY* photometry) is one of several now being used to search for lenses in the Dark Energy Survey (Agnello et al. 2015; Ostrovski et al. 2017), which ought to produce at least as many lensed quasars as ATLAS. As no one method will be perfect, comparison of the results will shed light on their relative strengths and weaknesses.

6.2. Lensless Twins

The VST-ATLAS survey has better seeing than SDSS, allowing, in principle, the discovery of less widely separated lensed quasars. The galaxies that produce close pairs are fainter than those that produce wide pairs. They are also more crowded by the lensed quasar images, making it more difficult to identify them.

While no lensing galaxy has been identified for either of our "lensless twin" quasars, we have argued that it is premature to classify either system as binary quasars—fraternal twins. In Figure 8 we show the two systems with the component spectra shifted to overlap. For WISE 0326-3122 the agreement is nearly perfect, while for WISE 1051-1142 the differences are consistent with what one would expect for a microlensed system. We note that WISE 2329-1258 was at first classified as a lensless twin system, but in the time since the original submission of this paper, it has been reclassified as a lensed quasar with the detection of a lensing galaxy by other investigators.

With sufficiently deep direct images in sufficiently good seeing, one can set upper limits on the lensing galaxy that rule out the lensing hypothesis, but only with extensive modeling of lensing scenarios. If spectra with higher signal-to-noise ratio or spectra at other wavelengths were to show significant differences in the line profiles, they would again rule out the lensing hypothesis. Confirmation of the lensing hypothesis might come either from identification of the lensing galaxy or from correlated variations in the fluxes, as might be obtained from synoptic observations with the LSST.

7. Summary

We have analyzed images from the VST-ATLAS survey to identify candidate gravitationally lensed quasar systems in a sample of *WISE* sources with $W1 - W2 > 0.7$. Results from follow-up spectroscopy with the Baade 6.5 m telescope are presented for eight systems. One of them is a quadruply lensed

quasar, and two are doubly lensed systems. Two are projected superpositions of quasars at two different redshifts, and one appears to be a pair of distinct quasars at the same redshift. In two systems the component spectra are consistent with the lensing hypothesis, after allowing for microlensing. But as no lensing galaxy is detected in these two sources, we classify them as lensless twins. More extensive observations are needed to establish whether they are lensed quasars or physical binaries.

References

Agnello, A., Treu, T., Ostrovski, F., et al. 2015, MNRAS, 454, 1260
Agol, E., & Krolik, J. 1999, ApJ, 524, 49
Blackburne, J. A., Pooley, D., Rappaport, S., & Schechter, P. L. 2011, ApJ, 729, 34
Courbin, F., Lidman, C., & Magain, P. 1998, A&A, 330, 57
Cross, N. J. G., Collins, R. S., Mann, R. G., et al. 2012, A&A, 548, A119
Dressler, A., Bigelow, B., Hare, T., et al. 2011, PASP, 123, 288
Hambly, N. C., Collins, R. S., Cross, N. J. G., et al. 2008, MNRAS, 384, 637
Hennawi, J. F., Strauss, M. A., Oguri, M., et al. 2006, AJ, 131, 1
Inada, N., Oguri, M., Shin, M.-S., et al. 2012, AJ, 143, 119
Jiménez-Vicente, J., Mediavilla, E., Kochanek, C. S., & Muñoz, J. A. 2015, ApJ, 799, 149
Keeton, C. R. 2001, arXiv:astro-ph/0102340
Kochanek, C. S., Falco, E. E., & Muñoz, J. A. 1999, ApJ, 510, 590
Lidman, C., Courbin, F., Kneib, J.-P., et al. 2000, A&A, 364, L62
More, A., Oguri, M., Kayo, I., et al. 2016, MNRAS, 456, 1595
Mortlock, D. J., Webster, R. L., & Francis, P. J. 1999, MNRAS, 309, 836
Ostrovski, F., McMahon, R. G., Connolly, A. J., et al. 2017, MNRAS, 465, 4325
Pooley, D., Blackburne, J. A., Rappaport, S., & Schechter, P. L. 2007, ApJ, 661, 19
Pooley, D., Rappaport, S., Blackburne, J. A., Schechter, P. L., & Wambsganss, J. 2012, ApJ, 744, 111
Rauch, K. P., & Blandford, R. D. 1991, ApJL, 381, L39
Remy, M., Claeskens, J.-F., Surdej, J., et al. 1998, NewA, 3, 379
Richards, G. T., Fan, X., Schneider, D. P., et al. 2001, AJ, 121, 2308
Schechter, P. L., Mateo, M., & Saha, A. 1993, PASP, 105, 1342
Schechter, P. L., & Wambsganss, J. 2002, ApJ, 580, 685
Schechter, P. L., & Wambsganss, J. 2004, in IAU Symp. 220, Dark Matter in Galaxies, ed. S. Ryder et al. (San Francisco, CA: ASP), 103
Sérsic, J. L. 1963, BAAA, 6, 41
Shanks, T., Metcalfe, N., Chehade, B., et al. 2015, MNRAS, 451, 4238
Stern, D., Assef, R. J., Benford, D. J., et al. 2012, ApJ, 753, 30
Treu, T., & Marshall, P. J. 2016, A&ARv, 24, #11
Wisotzki, L., Koehler, T., Ikonomou, M., & Reimers, D. 1995, A&A, 297, L59
Wisotzki, L., Koehler, T., Kayser, R., & Reimers, D. 1993, A&A, 278, L15
Witt, H. J., Mao, S., & Schechter, P. L. 1995, ApJ, 443, 18
Wright, E. L., Eisenhardt, P. R. M., Mainzer, A. K., et al. 2010, AJ, 140, 1868